

Inferences of all-sky solar irradiance using Terra and Aqua MODIS satellite data

R. HOUBORG*†, H. SOEGAARD†, W. EMMERICH‡ and S. MORAN‡

†Department of Geography, University of Copenhagen, Oester Voldgade 10, DK-1350, Copenhagen, Denmark

‡USDA-ARS Southwest Watershed Research Center, 2000 E. Allen Rd, Tucson, AZ 85719, USA

(Received 4 May 2006; in final form 21 November 2006)

Solar irradiance is a key environmental control, and accurate spatial and temporal solar irradiance data are important for a wide range of applications related to energy and carbon cycling, weather prediction, and climate change. This study presents a satellite-based scheme for the retrieval of all-sky solar irradiance components, which links a physically based clear-sky model with a neural network version of a rigorous radiative transfer model. The scheme exploits the improved cloud characterization and retrieval capabilities of the MODerate resolution Imaging Spectroradiometer (MODIS) onboard the Terra and Aqua satellites, and employs a cloud motion tracking scheme for the production of hourly solar irradiance data throughout the day. The scheme was implemented for the Island of Zealand, Denmark (56° N, 12° E) and Southern Arizona, USA (31° N, 110° W) permitting model evaluation for two highly contrasting climates and cloud environments. Information on the atmospheric state was provided by MODIS data products and verifications against AERosol RObotic NETwork (AERONET) data demonstrated usefulness of MODIS aerosol optical depth and total precipitable water vapour retrievals for the delineation of spatial gradients. However, aerosol retrievals were significantly biased for the semi-arid region, and water-vapour retrievals were characterized by systematic deviations from the measurements. Hourly global solar irradiance data were retrieved with overall root mean square deviations of 11.5% (60 W m^{-2}) and 26.6% (72 W m^{-2}) for Southern Arizona and the Island of Zealand, respectively. For both regions, hourly satellite estimates were shown to be more reliable than pyranometer measurements from ground stations only 15 km away from the point of interest, which is comparable to the accuracy level obtainable from geostationary satellites with image acquisitions every 15–30 min. The proposed scheme is particularly useful for solar irradiance mapping in high-latitude regions as data from geostationary satellites experience a gradual degradation in spatial resolution and overall quality with latitude and become unusable above approximately 60° latitude. However, in principle, the scheme can be applied anywhere on the globe, and a synergistic use of MODIS and geostationary satellite datasets may be envisaged for some applications.

*Corresponding author. Email: rmhouborg@gmail.com

1. Introduction

Surface solar irradiance is an important environmental control in exchange processes of energy and carbon dioxide between the terrestrial ecosystem and the atmosphere, and accurate solar irradiance data are essential for climate change research studies and for an improved understanding of water and carbon cycling.

Surface solar irradiance is characterized by significant fluctuations both spatially and temporally mainly due to variations in cloudiness, atmospheric conditions and the elevation of the Sun. The large spatial and temporal heterogeneity of solar irradiance limits the use of widely spaced ground observations in regional or global scale applications. Often, satellite data are the only source for a detailed knowledge of spatially and temporally distributed solar irradiance fields.

Numerous attempts at deriving surface solar irradiance using geostationary satellite data have been made using either semi-empirical statistical approaches (Cano *et al.* 1986) or physical radiative transfer schemes (Gautier *et al.* 1980, Pinker and Laszlo 1992). The global climatology of satellite-measured radiances made available under the International Satellite Cloud Climatology Project (ISCCP) was an important contributor to progress related to global-scale surface solar irradiance modelling in the 1990s (Bishop and Rossow 1991, Pinker and Laszlo 1992, Zhang *et al.* 1995), while more recent approaches took advantage of finer-resolution products from the Geostationary Operational Environmental Satellite (GOES) (e.g. Pinker *et al.* 1994, Diak *et al.* 1996, Gautier and Landsfield 1997, Stewart *et al.* 1999, Jacobs *et al.* 2002, Ceballos *et al.* 2004) and the Meteorological Satellite (METEOSAT) (e.g. Beyer *et al.* 1996, Ba *et al.* 2001, Perez *et al.* 2002, Rigollier *et al.* 2004). Common to all of these approaches is a fairly simple parameterization of cloud transmission based on an empirical or physical relationship between the surface albedo and the planetary albedo determined from satellite-estimated radiances. Investigators employing GOES or METEOSAT products have reported accuracies on the order of 10–30% for hourly and 10–15% for daily insolation estimates when compared with ground-based pyranometers.

The reasonable success of geostationary satellites for solar irradiance mapping stems from their high temporal resolution with image acquisitions every 15–30 min enabling diurnal monitoring of cloud movement and development, and the generation of time and site-specific irradiance data. Being positioned above the equator, the geostationary satellites view the Earth's surface at an increasing angle with increasing latitude causing a gradual degradation of spatial resolution and data reliability. As a consequence, the utility of geostationary satellites for solar irradiance mapping becomes highly questionable at high latitudes. Sun-synchronous polar orbiting satellites on the other hand are not affected by declined accuracy due to unfavourable scan angles and the frequency of overflights increases towards the Polar regions. In addition, they cover the entire globe at a uniform spatial resolution (at nadir).

Few studies have focused on the use of polar orbiting satellites for solar irradiance mapping, and they have primarily been based on data from the Advanced Very High Resolution Radiometer (AVHRR) on board the NOAA satellites (Laine *et al.* 1999, Key 2002). As one of the new generation of sensors, the MODerate resolution Imaging Spectroradiometer (MODIS) signifies substantial improvements in spatial resolution, number of spectral channels, radiometric calibration, and geometric quality (Kaufman *et al.* 1998). This state-of-the-art instrument carried onboard the Terra and Aqua Earth Observing System satellites provides the remote-sensing user

community with an enhanced set of derived atmospheric, terrestrial, and oceanic products. Solar irradiance modelling might benefit from the enhanced cloud-characterization capabilities that will permit the integrated use of accurate radiative transfer schemes using input of MODIS derived cloud physical and radiative parameters such as optical depth, particle radius, phase, and temperature. The new information provided on aerosol characteristics, columnar ozone, and water vapour could also prove useful for quantifying the attenuation of solar irradiance in time and space.

While the generation of temporally distributed solar irradiance fields based on MODIS imagery is impacted by the low temporal frequency of this sensor, the availability of a morning (Terra) and afternoon (Aqua) overpass permits the investigation of changes that occur over the course of the day such as the buildup or dissipation of clouds. The ability of the MODIS instruments to capture the temporal dynamics of parameters relevant for solar irradiance modelling increases with latitude with full daily coverage above approximately 30° latitude (Wolfe *et al.* 1998) and the availability of three or more overpasses during the daytime poleward of approximately 60° (<http://earthobservatory.nasa.gov/MissionControl/overpass.html>).

This study presents a scheme for retrieving all-sky surface solar irradiance components that exploits the new suite of atmospheric products generated by the MODIS science team. A physical method was employed for the estimation of spectrally resolved clear-sky solar irradiance components, while a neural network approximation of a rigorous radiative transfer model was adopted for cloudy situations. The scheme relies on the use of cloud properties derived from the late morning and afternoon MODIS overpass, and the usefulness of MODIS derived aerosol optical depth and precipitable water vapour data for describing the atmospheric state was evaluated. The derivation of hourly solar irradiance data was made feasible by employing cloud motion vectors for the tracking of cloud information observed at the MODIS overpass times in space and time. The scheme was implemented for the Island of Zealand, Denmark (56° N, 12° E) and Southern Arizona, USA (31° N, 110° E) characterized by highly contrasting climates and cloud environments, and extensively verified against pyranometer measurements.

To the best of our knowledge, the utilization of MODIS data products for the purpose of solar irradiance mapping has not been done before, and this analysis can provide an insight into the usefulness of the suite of atmospheric and cloud parameters produced by the MODIS science team. The limited applicability of data from geostationary satellites in high latitudes makes this study highly relevant for the accurate retrieval of surface solar irradiance in these areas. Additionally, a synergetic use of polar orbiting and geostationary satellites may be envisaged for lower-latitude regions.

1.1 Study site and ground measurements

The model was implemented and tested for two regions characterized by highly contrasting climates and cloud environments (figure 1(a) and (b)). Southern Arizona in Southwestern USA (31° N, 110° E) is a semi-arid environment with a monsoon season that occurs during the months of July to September as the winds shift to a southerly and south-easterly direction pulling moisture from the Pacific Ocean and the Gulf of Mexico northward. The 30-year average precipitation is around 300 mm. The Island of Zealand, Denmark (56° N, 12° E) is located in the zone of prevailing westerlies, which causes a temperate and fairly humid environment with a yearly

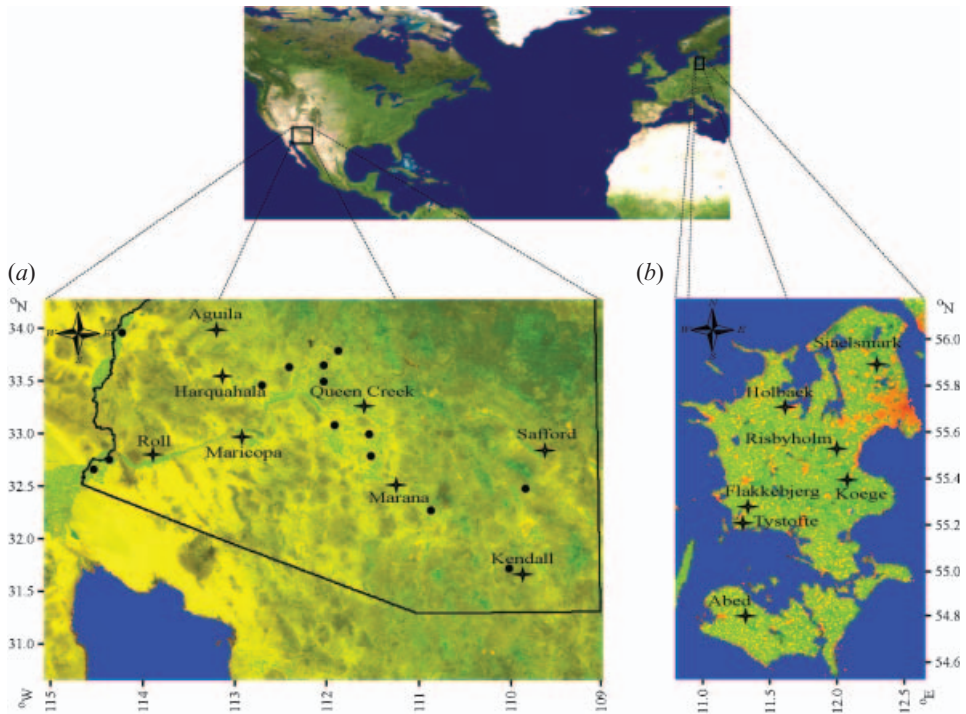


Figure 1. Study regions with names and location of meteorological towers. (a) Southern Arizona, USA. The dots indicate the position of measurement towers used along with the validation sites (stars) to assess the spatial variability in global solar irradiance within the study region (§3.3). The smallest distance between network sites is 10 km. (b) The Island of Zealand, Denmark. The smallest distance between network sites is between the Flakkebjerg and Tystofte meteorological towers (9.4 km). The images are true-colour composites of the MODIS near-infrared and red reflectance bands for day of year 161.

precipitation total of approximately 700 mm. The most striking difference is the frequency of clear-sky conditions with percentages of possible sunshine of almost 85% in Southern Arizona and only 35% in Denmark (Denmark's Meteorological Institute 2006).

Global solar irradiance simulations for Southern Arizona were verified against ground observations from 2003 acquired from meteorological stations operated by the Arizona Meteorological Network (AZMET) and from sites within the Walnut Gulch Experimental Watershed maintained by the Southwest Watershed Research Center (SWRC) (figure 1(a)). The AZMET stations are all equipped with LI-COR LI200S pyranometers that are sampled every 10 s and summed to produce hourly global irradiance values in units of MJ m^{-2} . The stations within Walnut Gulch are equipped with LI-COR LI200X pyranometers, sampled every 2 s (W m^{-2}) and the average recorded in 20-min intervals. For the Island of Zealand, pyranometer validation data for 2004 were acquired from meteorological stations operated by Denmark's Meteorological Institute (DMI) and from the Risbyholm flux tower site operated by the Department of Geography, University of Copenhagen (figure 1(b)). All DMI stations are equipped with STAR pyranometers sampled every 10 s and the average recorded in hourly intervals. The Risbyholm station is equipped with a Delta-T BF3 sunshine sensor and employs a similar sampling strategy. All stations

are carefully monitored, and solar sensors replaced with recalibrated sensors on a yearly basis.

2. Methodology

Satellite and weather prediction data are presented in §2.1. A description of the surface solar irradiance models is given in §2.2, after which the satellite-based scheme for the retrieval of all-sky solar irradiance components is outlined.

2.1 *Satellite and weather prediction data*

Terra and Aqua MODIS data products (§2.1.1) were acquired from the EOS Data Gateway (<http://delenn.gsfc.nasa.gov/~imswww/pub/imswelcome/>). For the present application and model testing, the MODIS data acquisition was limited to days with the availability of two overpasses—one late morning (Terra) and one afternoon (Aqua) overpass. However, the scheme may also be run with the availability of only one scene during the daytime enabling solar irradiance computations for all 365 days poleward of approximately 30° (Wolfe *et al.* 1998). All MODIS swath data (MOD/MYD04/05/06/07) were geo-registered using latitude and longitude geometry bands from the geolocation dataset (MOD/MYD03), while the albedo product (MOD43) is distributed in a sinusoidal grid projection (SIN). All scenes were geometrically rectified to UTM coordinates (UTM zone 12, Datum North America 1983 or UTM zone 32, Datum European 1950). The geolocated MODIS data are provided at a sub-pixel accuracy, with a geolocation accuracy of approximately 50 m at nadir (Wolfe *et al.* 2002).

Atmospheric motion vectors for the Island of Zealand (§2.1.2) were provided in GRIB format by the European Center for Medium-range Weather Forecasting (ECMWF) and decoded using the program wgrib made available by the Climate prediction Center (<http://www.cpc.ncep.noaa.gov/products/wesley/wgrib.html>). Cloud motion vectors for Southern Arizona were acquired from GOES-10 cloud-drift products (§2.1.2) made available by the NOAA National Climatic Data Center (NCDC).

2.1.1 MODIS data. Spatial information on cloud and atmospheric properties was acquired from Terra and Aqua MODIS science data sets comprising the aerosol product (MOD/MYD04), the total precipitable water product (MOD/MYD05), the cloud product (MOD/MYD06), and the atmospheric profiles product (MOD/MYD07).

Aerosol properties are reported at 10-km resolution in MOD04 and are derived by inversion of MODIS observed reflectances at 500-m resolution using precomputed radiative transfer look-up tables generated by dynamical aerosol models (Kaufman *et al.* 1997). The near-infrared retrieval algorithm for the total precipitable water vapour employs MODIS water-vapour absorption and atmospheric window bands for inferences of atmospheric water-vapour transmittances that are converted to total column water vapour at 1-km resolution using precalculated lookup tables (Kaufman and Gao 1992). Cloud optical properties like the optical thickness and the particle effective radius are derived at 1-km resolution using a combination of visible and near-infrared MODIS bands, while cloud top properties and thermodynamic phase are produced at 5-km resolution using thermal bands and longwave CO₂ absorption bands (Platnick *et al.* 2003). Integrated quantities such as the total column ozone and total precipitable water

vapour (infrared retrieval) are reported at 5-km resolution in MOD/MYD07 using a statistical retrieval algorithm that employs 12 MODIS infrared bands (Menzel *et al.* 2002).

Additionally, 16-day representations of the directional hemispherical reflectance ('black-sky albedo') and bihemispherical reflectance ('white-sky albedo') were acquired from the MODIS BRDF and albedo product (MOD43) for the determination of the broadband surface albedo. The BRDF algorithm relies on multirate, clear sky, and atmospherically corrected observations, but in case of insufficient high-quality reflectance data within the 16-day interval, the albedo retrievals rely on a less accurate backup algorithm.

All acquired MODIS data products are version 4.0 high-quality validated products suitable for scientific studies. Product MOD/MYD04 and MOD/MYD05 are currently in a stage 2 validation (3 represents the highest degree of product confidence), while the remaining products are in a stage 1 validation. MODIS total ozone retrievals have been shown to compare favourably with retrievals from the GOES-8 Sounder and the Earth Probe TOMS (Total Ozone Mapping Spectrometer) (<http://modis-atmos.gsfc.nasa.gov/>) and MODIS albedos have been validated to maximum errors of 5% (<http://landval.gsfc.nasa.gov/MODIS/index.php>). Limited validation information exists on the accuracy of the MODIS cloud information (<http://modis-atmos.gsfc.nasa.gov/validation.html>) due to the lack of extensive *in situ* measurements. The performance of the cloud product partly depends on the MODIS cloud detection capabilities that rely on an enhanced set of algorithms employing a series of spectral threshold and confidence tests based on 14 bands in the visible and infrared spectral region (Ackerman *et al.* 1998). Validation results for MODIS retrievals of aerosol optical depth and total precipitable water vapour are presented in §3.2.

2.1.2 GOES and ECMWF data. Spatial and temporal fields of cloud wind speed and direction are required as input to the model in order to extrapolate the MODIS instantaneous cloud information to a diurnal timescale (§2.3.3). In the present application, information on the cloud motion was taken from two sources, namely the NOAA/NESDIS operational cloud drift product (Nieman *et al.* 1997) and the ECMWF reanalysis product.

The NOAA/NESDIS cloud motion vectors are automatically generated with a frequency of 3 h by tracking homogeneous cloud masses in a sequence of three GOES images. Targeting boxes with a resolution of 15×15 pixels are used to detect and track the cloud masses, and the cloud motion vectors are derived in an irregular spatial pattern dependent on the distribution of the clouds. A grid spacing of 30 km was employed for the present application. RMS deviations ranging from 5.0 to 5.5 m s^{-1} have been reported from comparisons between GOES cloud drift vectors and co-located radiosondes (Menzel 2001).

Atmospheric motion vectors from ECMWF are provided at six-hourly intervals, at a grid-size of 0.5° and at 21 pressure levels ranging from 1 to 1000 mb. ECMWF atmospheric motion vectors extracted from the pressure level closest to the MODIS-derived cloud top pressure were used as an approximation of the cloud motion.

2.2 Surface solar irradiance models

A fast neural network approximation of a rigorous radiative transfer model was adopted for simulations of broadband global solar irradiance during cloudy

conditions (§2.2.2). While the same model is capable of performing solar irradiance computations during clear-sky situations, a more flexible scheme was employed for these situations, enabling the computation of spectrally resolved direct-beam and diffuse solar irradiance components (§2.2.1). The input requirements of the two schemes are listed in figure 2. In addition, the solar elevation was calculated using the accurate astronomical algorithms published by Meeus (1991).

2.2.1 Clear-sky module. The simple clear-sky solar spectral model by Bird and Riordan (1986) was adopted for the simulation of spectrally resolved direct and diffuse irradiance components on horizontal and tilted planes. The model code (Spectrl2) was provided by the National Renewable Energy Laboratory (<http://rredc.nrel.gov>).

In the model, the direct-beam irradiance on a horizontal surface for wavelength λ is formulated as

$$I_b(\lambda) = E_0 I_{sc}(\lambda) T(\lambda) \cos(\theta_z).$$

The parameter E_0 is an eccentricity correction factor that is given as a function of the day of year, θ_z is the Sun zenith angle, $I_{sc}(\lambda)$ is the wavelength-dependent extraterrestrial irradiance at the mean Earth–Sun distance, and T is the total atmospheric transmittance. T is given as the multiplicative of the transmittance functions for Rayleigh scattering of air molecules, scattering and absorption by aerosols, water-vapour absorption, ozone absorption, and mixed gas absorption, respectively. The diffuse irradiance component on a horizontal surface is formulated

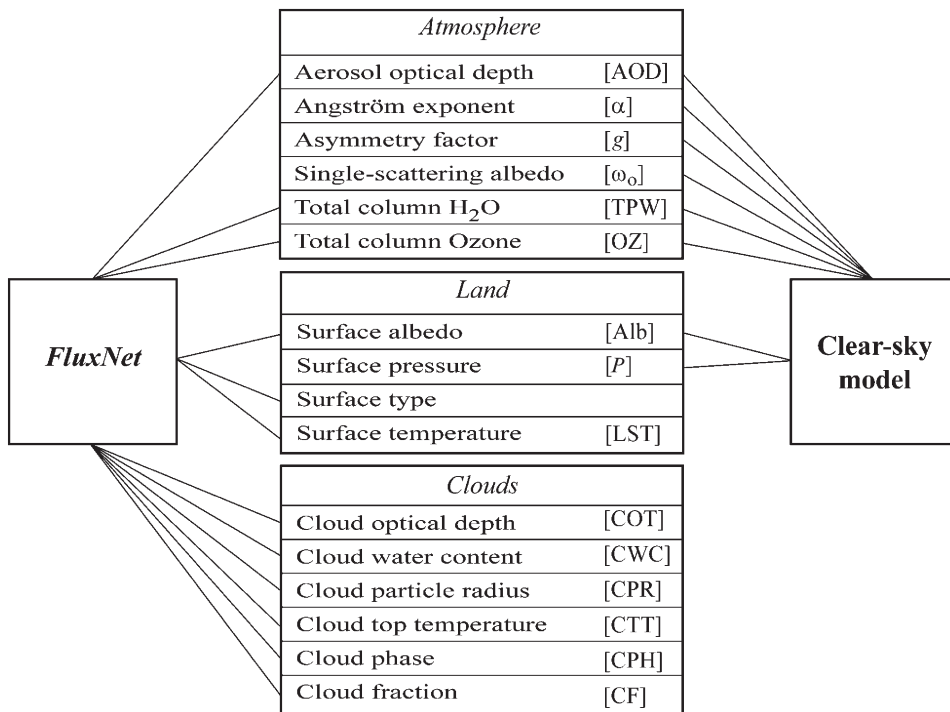


Figure 2. Overview of required input parameters for the FluxNet and clear-sky solar irradiance models.

as the sum of Rayleigh-scattered, aerosol-scattered, and multiply reflected diffuse irradiance, respectively, using modifications of the expressions in Justus and Paris (1984).

The single-scattering albedo (at $0.4\ \mu\text{m}$) (ω_0) and the asymmetry factor (g) required as input to the model (figure 2) are very difficult to determine accurately, given their dependence on the material, shape, size, and optical properties of aerosols. For the present application, ω_0 and g were parameterized according to the Standard Radiation Atmosphere (SRA) aerosol model from IAMAP (1986) that distinguishes between continental (rural), urban, and maritime aerosol types.

The model operates with 122 wavelengths ranging from 0.3 to 4.0 nm and was set up to produce broadband photosynthetically active (0.3–0.7 nm), near-infrared (0.7–4.0 nm), and solar (0.3–4.0 nm) irradiance by integration over the specified bandwidths.

2.2.2 Cloudy-sky module. Simulations during cloudy skies were performed using *FluxNet*, which is a neural network approximation of the radiative transfer model *Streamer* (Key and Schweiger 1998). The model code for *FluxNet* (version 4.0) is provided at <http://stratus.ssec.wisc.edu/FluxNet/FluxNet.html>.

Streamer calculates irradiance fluxes or radiances for a wide variety of surface and atmospheric conditions using the DISORT (Stamnes *et al.* 2000) discrete ordinate solver. Spectrally resolved fluxes are computed in *Streamer* with 24 shortwave and 105 longwave bands, which are consolidated into one shortwave and one longwave band in *FluxNet* for broadband computations.

In *Streamer*, cloud properties can be specified with a high degree of flexibility and detail with up to 50 individual cloud types and cloud layers for each scene/pixel. In *FluxNet*, each scene can consist of only one cloud layer, and the number of input parameters has been significantly reduced (figure 2). However, *FluxNet* is 100–100 000 times as fast as *Streamer*, making it more feasible for satellite applications.

While land surface temperature (LST) and emissivity are important inputs to *FluxNet* for simulations of longwave fluxes, they have a minor effect on the amount of solar irradiance received at the surface. Consequently, the land surface emissivity was fixed to a value of 0.98, whereas LSTs were acquired from the MODIS cloud product (MOD/MYD06) that record LSTs produced by the National Center for Environmental Prediction (NCEP). The surface type (vegetation, water, snow) was assessed from the land mask associated with MOD05.

FluxNet estimates of global solar irradiance were input into the diffuse fraction model of Skartveit *et al.* (1998) for the separation of the diffuse component. The model considers the effect of variable and inhomogeneous clouds on the diffuse fraction, and despite the empirical nature of the model, it has been shown to perform satisfactorily in widely different climatic regions (Skartveit *et al.* 1998).

In principle, *FluxNet* can be applied globally, as the dataset used to train the network covers all latitudes. Comparisons of *FluxNet* and *Streamer* results of incoming shortwave radiation yield a bias of $-0.05\ \text{W m}^{-2}$ and RMS deviations of around $18\ \text{W m}^{-2}$ (Key *et al.* 2001).

2.3 All-sky solar irradiance retrieval scheme

An overview of the satellite-based all-sky solar irradiance retrieval scheme is given in figure 3(a)–(c). Cloud, land, and atmospheric parameters were acquired from Terra and Aqua MODIS data products (§2.1.1), and a cloud-tracking technique, utilizing

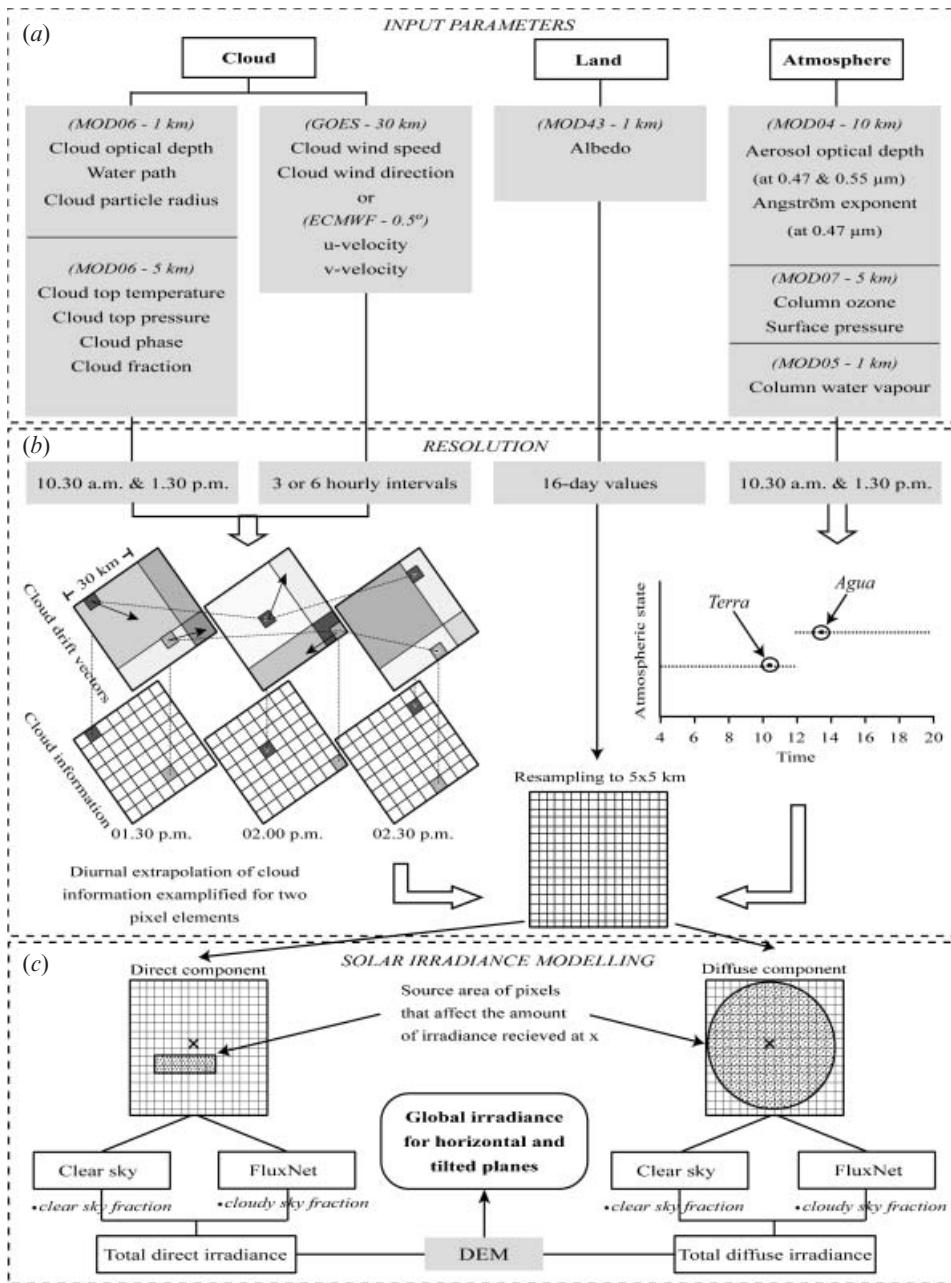


Figure 3. Satellite-based scheme for the retrieval of all-sky solar irradiance components. (a) Satellite derived inferences of cloud, land, and atmospheric input parameters. (b) Temporal and spatial interpolation and extrapolation of MODIS atmospheric state and cloud parameters. (c) Solar irradiance modeling approach with consideration of the pixel-Sun geometry and the different directional properties of direct-beam and diffuse irradiance.

GOES or ECMWF cloud motion vectors (§2.1.2), is a key element in the scheme as it allows for the temporal extrapolation of cloud information observed at the Terra and Aqua overpass times to the entire day (§2.3.3). The scheme considers the

pixel–Sun geometry and performs a spatial averaging of MODIS input parameters within computed source areas of direct-beam and diffuse solar irradiance for each pixel (§2.3.4).

2.3.1 Spatial resampling. All input parameters were resampled to a common pixel size of 5×5 km. The 1-km-resolution cloud optical parameters, the total precipitable water vapour, and the surface albedo were resampled to the 5-km grid size using a pixel-aggregation technique. The 10×10 km resolution aerosol product was assumed spatially homogeneous at the sub-pixel scale allowing the same 10-km grid value to be used in the four sub-grids. The GOES cloud-drift and the ECMWF atmospheric motion products were resized to the 5×5 km pixel resolution in a similar way.

2.3.2 Temporal and spatial extrapolation and interpolation. The observations of the atmospheric clear-sky parameters at the overpass times (≈ 10.30 a.m. and ≈ 1.30 p.m.) were fixed for the remainder of the day, assuming a sufficient description of the diurnal course in the atmospheric state between sunrise and sunset from two daily observations (figure 3(b)). Atmospheric state parameters reported for clear-sky pixels were extended to the entire region using a spatial interpolation technique. However, a spatially interpolated value may not be representative of local atmospheric conditions when the nearest cloud-free pixel is far away. As a result, a seasonal climatology of each clear-sky parameter was established in grids of 100×100 km on the basis of all MODIS scenes containing valid data within each 100 km grid throughout the year. Subsequently, cloud-contaminated pixels located more than 100 km away from a valid clear-sky data pixel were assigned a value on the basis of the produced local MODIS climatology rather than the nearest clear sky pixel value. The exact value was calculated as the interpolated value between the two closest data-containing overpasses.

The daily variation in the surface albedo was approximated by linearly interpolating the black-sky and white-sky albedos between the midpoints of each 16-day observation interval. As the black-sky and white-sky albedos mark the extreme cases of completely direct and completely diffuse illumination, surface albedos for given atmospheric conditions were estimated by weighting the interpolated black-sky and white-sky albedos with the fraction of diffuse skylight. This procedure should provide reasonable daily estimates for surfaces undergoing minor changes in surface characteristics throughout the 16-day period.

2.3.3 Cloud-tracking scheme. Whereas it is reasonable to assume constant values of clear-sky atmospheric parameters on a daily timescale, high-temporal-resolution cloud information is essential as cloud fluctuations throughout a day can have a large effect on the diurnal course in solar irradiance. GOES and ECMWF inferred cloud-drift vectors (§2.1.2) were employed to track cloud information (COT, CWC, CPR, CTT, CPH, CF) observed at the Terra and Aqua overpasses in time and space for Southern Arizona and the Island of Zealand, respectively. The methodology is schematized in figure 3(b) for two pixel elements between the Aqua overpass time and 2.30 p.m. First, the cloud drift vectors were reproduced at half-hourly time steps by linearly interpolating between the three- or six-hourly predictions. The cloud-drift vectors at the Aqua overpass time were then used to track the cloudy pixel elements in the Aqua overpass images to their pixel positions 30 min after the overpass creating new maps of spatially distributed cloud information. Subsequently, cloud-drift vectors 30 min after the Aqua overpass were applied to

the cloudy pixel elements in the new maps, creating a new set of images approximating the distribution of cloud information 1 h after the overpass. A continuation of this methodology allowed for a temporal extrapolation of the respective cloud parameters in half-hour intervals between the Aqua overpass time and sunset. A similar approach was employed between the Terra overpass and sunrise by using the reflections of the cloud drift vectors to backtrack the cloud information.

Evidently, errors in the cloud-drift vectors will affect the ability of the scheme to accurately predict the position of the individual pixel elements in time and space. Inaccurate spatial positioning of cloud information will particularly affect the direct component of solar irradiance due to the relatively small pixel source area (§2.3.4), and errors will tend to propagate the further away one is from the overpass time. Deviations between plot measurements and satellite predictions are expected to maximize during broken cloud conditions dominated by scattered optically thick cloud elements as the prediction of the position of individual cloud elements would have to be very precise for accurate solar irradiance modelling at the plot scale. Moreover, as the implicit assumption of complete shape coherence of the cloud masses is tenable over shorter time intervals, the extrapolation technique is expected to be most successful for time intervals close to the satellite overpasses. As the time from the satellite overpasses increases, growth, dissipation, or disintegration of cloud masses may become important.

2.3.4 Solar irradiance modelling with consideration of the pixel–Sun geometry. The pixel–Sun geometry was taken into consideration to make derived solar irradiance estimates more representative of each pixel locality. The different directional properties of direct-beam and diffuse irradiance cause the source area of pixels that affect the amount of irradiance received at a specific pixel to differ widely between the two components (figure 3(c)). For the direct-beam component, the pixel source area was constructed as a function of the solar zenith angle, the solar azimuth angle, and the cloud height and thickness (figure 4). The size of the source area will increase with increasing Sun zenith angle and cloud thickness. As irradiance computations were performed in half-hour intervals, the entire pixel source area over the half-hour interval was considered (figure 3(c)). The cloud and atmospheric parameters were averaged within the source area, and the effective values used as input for the direct-beam computation.

The pixel source area affecting the amount of diffuse irradiance received at a given pixel was estimated by assuming an equal hemispheric contribution of diffuse irradiance. The radius of the source area (figure 3(c)) was computed by setting the Sun zenith angle to a value of 87° and using a mean cloud height for the entire region. Effective values of the cloud and atmospheric parameters within the diffuse source area were calculated by weighting the values of each pixel element in the source area as a function of their distance from the centre pixel.

The clear-sky and *FluxNet* models were then run with the effective cloud and clear-sky atmospheric parameters, and the outputs were weighed by the effective clear-sky and cloudy-sky fractions in order to predict the total direct-beam and diffuse irradiance for all-sky situations. The direct-beam component during cloudy conditions was approximated as the difference between the *FluxNet* estimate of global solar irradiance and the diffuse irradiance output from the diffuse fraction model (§2.2.2). The global irradiance on tilted planes can be simulated with the additional input of the surface slope and aspect angle from a Digital Elevation

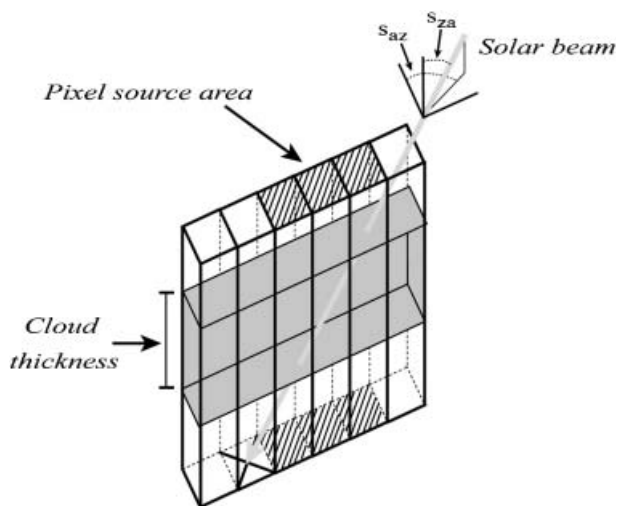


Figure 4. Illustration of the determination of the pixel source area for direct-beam irradiance received at a given 5×5 km pixel locality. At this specific combination of Sun zenith angle (S_{ZA}), azimuth angle (S_{AZ}), and cloud thickness, the atmospheric and cloud properties of *three pixels* affect the amount of solar irradiance received at the specific pixel locality. Since the illustration depicts an instantaneous view of the source area, it is only a fraction of the entire half-hourly source area used in the computation of the direct-beam component of global solar irradiance.

Model (DEM) using the simple scheme outlined by Bird and Riordan (1986). Computations for tilted planes are run at the spatial resolution of the DEM.

3. Results and discussion

In this section, a sensitivity analysis is employed to establish the importance of the input parameters of the *FluxNet* and clear-sky models for global solar irradiance retrievals (§3.1) and the reliability of MODIS atmospheric state data are evaluated by comparison with ground observations (§3.2). Then, model results are verified against ground pyranometer measurements (§3.3) after which sources of uncertainty are discussed (§3.4).

3.1 Sensitivity analysis

A sensitivity analysis was employed to establish the importance of the input parameters of the *FluxNet* and clear-sky models for global solar irradiance retrievals. In order to study the sensitivities over the whole range of variation of each parameter, the effect of an input parameter was evaluated at six levels representing a realistic range of variation. For this purpose, the solar irradiance models were run at each parameter level using all possible combinations of the remaining parameter settings (table 1).

Figure 5(a) and (b) compare the difference between the nominal run and sensitivity run results and show the mean change in solar irradiance for cloudy and clear sky conditions, respectively, caused by increasing the values individually for each of the model parameters. The error bars illustrate the standard deviation of the solar irradiance deviation response caused by input variations in the remaining model parameters. Not surprisingly, COT is seen to be the prime factor controlling

Table 1. Level values of the *FluxNet* and clear-sky model parameters used for the sensitivity simulations.

Parameters	Range	Levels (nominal run)	Levels (sensitivity run)
COT (–)	(*) 0–90	0, 15, 30, 45, 60, 75	+15
	(†) 0–45	0, 7.5, 15, 22.5, 30, 37.5	+7.5
CWC (g m ^{–3})	(*) 0.05–0.5	0.05, 0.125, 0.2, 0.275, 0.35, 0.425	+0.075
	(†) 0.0007–0.11	0.0007, 0.019, 0.037, 0.055, 0.073, 0.091	+0.018
CPR (μm)	(*) 3–21	3, 6, 9, 12, 15, 18	+3
	(†) 10–76	10, 21, 32, 43, 54, 65	+11
CTT (K)	(*) 253–298	253, 261, 268, 276, 283, 291	+7.5
	(†) 228–273	228, 236, 243, 251, 258, 266	+7.5
ALB (–)	0.15–0.55	0.15, 0.22, 0.28, 0.35, 0.42, 0.49	+0.067
AOD (–)	0.05–0.8	0.05, 0.175, 0.3, 0.425, 0.55, 0.675	+0.125
PWC (cm)	0.1–5.0	0.1, 0.9, 1.7, 2.6, 3.4, 4.2	+0.82
<i>g</i>	0.5–0.9	0.5, 0.57, 0.63, 0.7, 0.77, 0.83	+0.067
ω_0	0.6–1.0	0.6, 0.67, 0.73, 0.8, 0.87, 0.93	+0.067
OZ (g m ^{–2})	6.4–9.7	6.4, 7, 7.5, 8.1, 8.6, 9.2	+0.55
<i>P</i> (mb)	800–1100	800, 850, 900, 950, 1000, 1050	+50
α (–)	0.5–2.5	0.5, 0.75, 1, 1.25, 1.5, 2	+0.25

As the level values and ranges of some of the *FluxNet* parameters vary with cloud phase a sensitivity analysis was performed separately for liquid and ice clouds, respectively. The abbreviations are explained in figure 2. Constant values were used for the surface emissivity (0.98), temperature (293 K), and type (vegetation). The values listed in the last column must be added to the levels of the nominal run to get the levels of the sensitivity run.

**Liquid water cloud.*

†*Ice cloud.*

the amount of solar irradiance reaching the surface, and an average solar irradiance decrease of approximately 60% is the result of changing COT from 0 to 15 (figure 5(a)). For cloudy atmospheres, variations in cloud water (CWC) and ozone content (OZ) have a minimal effect on the solar irradiance, while somewhat greater sensitivities are observed for the cloud particle radius (CPR) (for ice clouds), aerosol optical depth (AOD), and surface albedo (ALB).

For clear sky conditions, AOD is the predominant factor influencing solar irradiance with a marked dependence on the Sun zenith angle (figure 5(b)). An increased sensitivity with increasing Sun zenith angle (S_{ZA}) is characteristic for all variables as the solar radiation has to pass through a much thicker atmosphere at low Sun angles causing greater scattering and absorption. Global solar irradiance is also seen to be sensitive to the aerosol type parameterization (g and ω_0) and the total precipitable water vapour (TPW). For dry atmospheres, an increase in TPW of 0.82 translates into a solar irradiance decrease of approximately 8% (figure 5(b)).

3.2 Verification of MODIS atmospheric state data

Uncertainties in the aerosol optical depth (AOD) and precipitable water vapour content (TPW) can have large implications for the accuracy of solar irradiance estimates during clear-sky conditions (figure 5(b)). An evaluation of MODIS AOD and TPW retrieval accuracies for the study regions was conducted by comparing the MODIS retrievals to level 2.0 AEROSOL ROBOTIC NETWORK (AERONET) data (Holben *et al.* 1998) from the Maricopa (33.07° N, –111.97° W) and Gotland

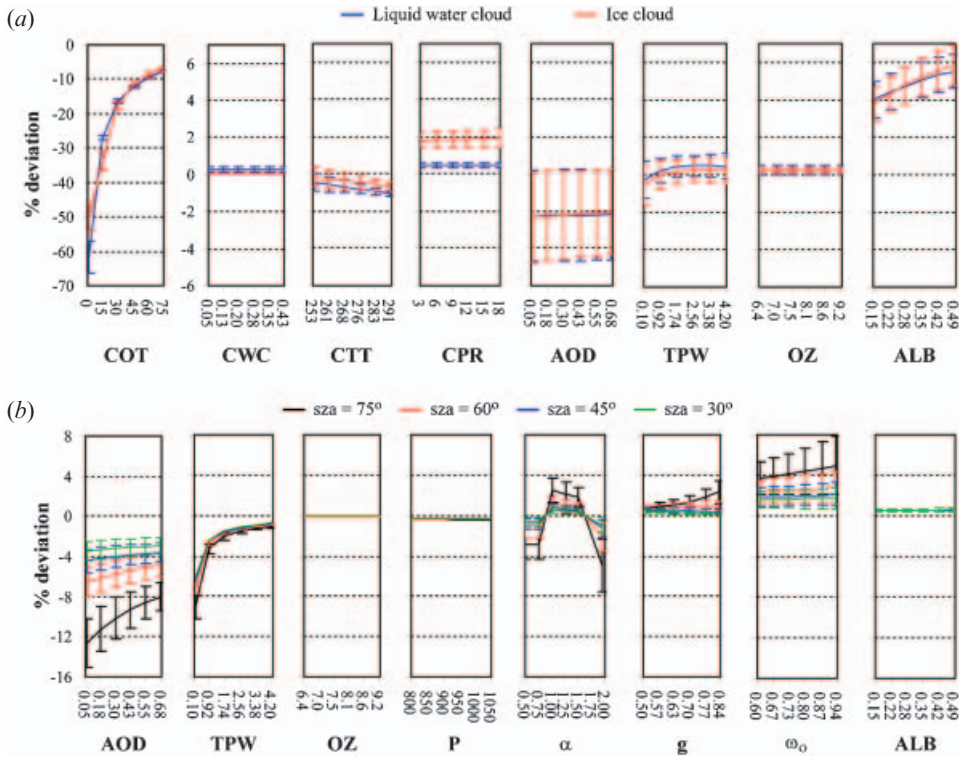


Figure 5. Sensitivities of global solar irradiance to stepwise changes in the input parameters of the *FluxNet* (a) and clear-sky model (b). The figures illustrate the mean change in solar irradiance at six levels for each input parameter (table 1) evaluated by running the models with all possible combinations of the remaining parameter levels. The sensitivity analysis was performed separately for liquid water and ice clouds but only the liquid water cloud ranges are displayed (a) (table 1 for the ice cloud ranges). For clear-sky conditions, the dependence on the Sun zenith angle (S_{ZA}) is given. The error bars show the standard deviation of the solar irradiance deviation response caused by input variations in the remaining model parameters. For the *FluxNet* simulations, the Sun zenith angle was set equal to 45° . The abbreviations are explained in figure 2.

(57.92° N, 18.95° E) sites, where the latter is the AERONET site in closest proximity to the Island of Zealand. Correlative datasets for the Swedish Gotland site were acquired from the MODIS Atmosphere Parameters Subset Statistics (MAPSS) database (http://modis-atmos.gsfc.nasa.gov/validation_corrdata.html). MODIS data were extracted from the closest pixel and screened for possible cloud contamination and compared with available AERONET measurements within 30 min of each MODIS overpass.

Evidently, MODIS AOD retrievals are highly problematic for the Maricopa site (figure 6(a)) with prediction accuracies much lower than the accuracy of $\pm 0.05 \pm 0.20 \cdot \text{AOD}$, predicted prior to launch (indicated by the two dotted lines). The poor performance for this site is probably related to a violation of the assumptions of the MODIS aerosol retrieval algorithm that tends to work best for dark, vegetated pixels (Kaufman *et al.* 1997). However, though significantly biased, the estimates still correlate with AERONET measurements ($R^2=0.82$), indicating a usefulness of the data for interpreting spatial gradients in AOD (figure 6(a)). A

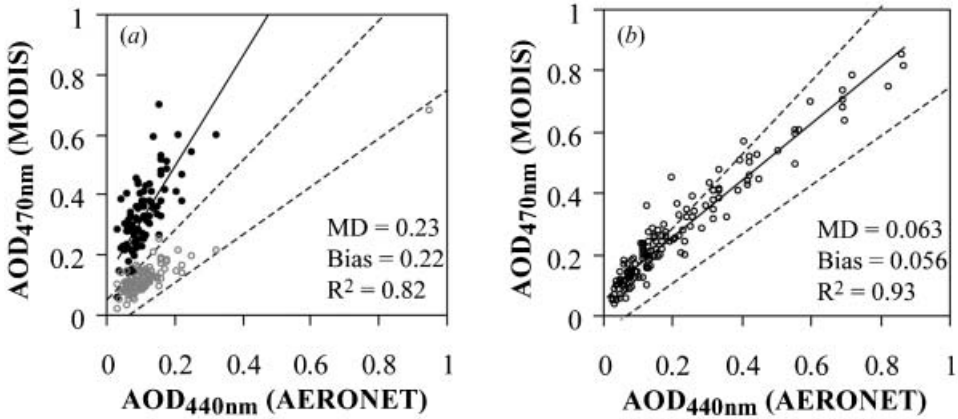


Figure 6. Verification of Terra MODIS derived aerosol optical depths (AOD) at 470 nm against AERONET sun photometer measurements from the Maricopa (a) and Gotland (b) sites based on data from 2003 (Maricopa) and 2002 (Gotland). The black lines are regression lines, and the two dotted lines indicate the MOD/MYD04 product accuracy predicted prior to launch ($\pm 0.05 \pm 0.2 \cdot \text{AOD}$). MD is the mean deviation. In (a), the hollow circles represent AOD retrievals corrected for the bias.

much higher AOD retrieval accuracy is observed for the Gotland site (figure 6(b)), but still the MODIS data tend to overestimate the Sun photometer measurements especially at small optical depths. Higher retrieval accuracies were reported by Vermote *et al.* (2002), who suggested a product accuracy of $\pm 0.05 \pm 0.1 \cdot \text{AOD}$ based on a small dataset for Maryland, USA. In a recent study by Remer *et al.* (2005), based on an extensive number of MODIS aerosol retrievals collocated with AERONET measurements, one standard deviation of MODIS AODs were reported to fall within the uncertainty predicted prior to launch.

While Terra MODIS TPW values based on the near-infrared retrieval algorithm and AERONET measurements are highly correlated at both sites (figure 7(a) and (b)), the MODIS predictions are systematically larger at the Maricopa site and systematically lower at the Gotland site with overall bias deviations of 20% and -9%, respectively. These trends were also observed for the Aqua dataset (not shown). The observed mean deviations are higher than the 5–10% range reported as the typical error in the MODIS near-infrared water vapour values (Gao and Kaufman 2003, King *et al.* 2003).

As a comparison, TPW values based on the integration of water vapour profiles (infrared retrieval) are only slightly biased (figure 8(a) and (b)) but less correlated with the surface measurements. Still reasonable agreements are observed for both sites with mean deviations of around 20% comparable to the accuracy reported by Seemann and Li (2003). Similar accuracies were observed for the Aqua dataset of infrared retrieved TPW (not shown). The greater scatter in the infrared retrievals may be explained by the reduced sounding capabilities of MODIS compared with real sounding instruments like the Atmospheric Infrared Sounder (AIRS) or the GOES sounder in addition to the statistical nature of the method that may suffer from inadequate global training data (Seemann and Li 2003). The near-infrared TPW retrievals were used in the solar irradiance scheme as they provide a much better delineation of horizontal gradients in water vapour compared with the infrared retrievals.

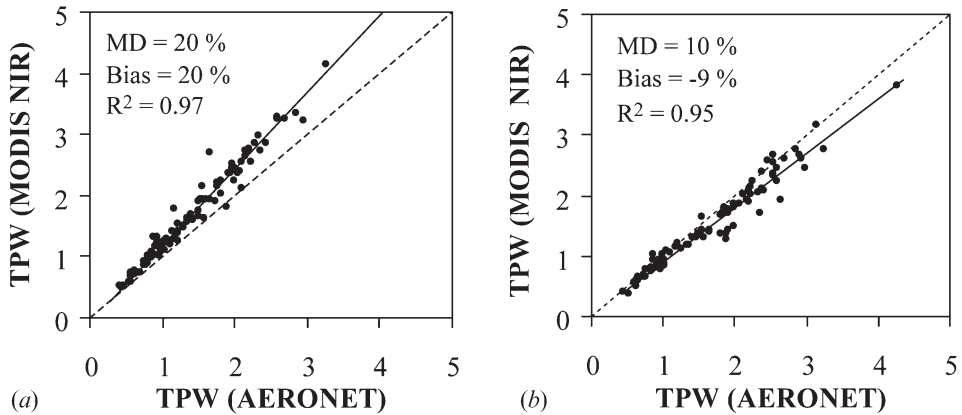


Figure 7. Comparisons of MODIS derived total precipitable water vapor (TPW) values, based on the near-infrared retrieval algorithm, and AERONET measurements from the Maricopa (a) and Gotland (b) sites based on data from 2003 (Maricopa) and 2002 (Gotland). The solid line is the regression fit, and the dotted line is the 1:1 line. MD is the mean deviation.

3.3 Global solar irradiance verification and evaluation

Figure 9 exemplifies the performance of the global solar irradiance simulations during variable degrees of cloud cover for the Kendall (figure 9(a)) and Koege (figure 9(b)) validation sites. Despite the difficulties and uncertainties associated with cloud tracking and radiative transfer modelling for cloudy atmospheres, the general trends in the solar irradiance are well established by the model results for these cases. In fact, many of the dips and peaks in the global solar irradiance are closely approximated by the model results.

The performance of the entire global solar irradiance dataset for the two study regions was evaluated by comparing the dataset with hourly pyranometer measurements from the validation sites indicated on figure 1. The half-hourly

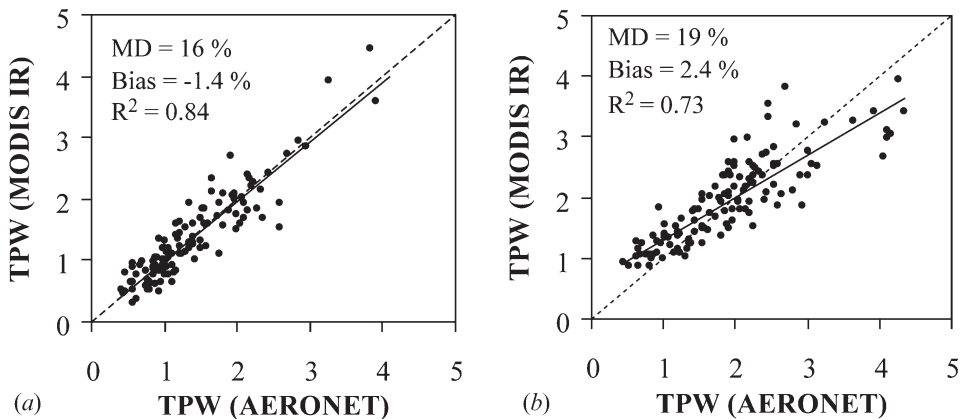


Figure 8. Comparisons of MODIS derived total precipitable water-vapor (TPW) values, based on the infrared retrieval algorithm, and AERONET measurements from the Maricopa (a) and Gotland (b) sites based on data from 2003 (Maricopa) and 2002 (Gotland). The solid line is the regression fit, and the dotted line is the 1:1 line. MD is the mean deviation.

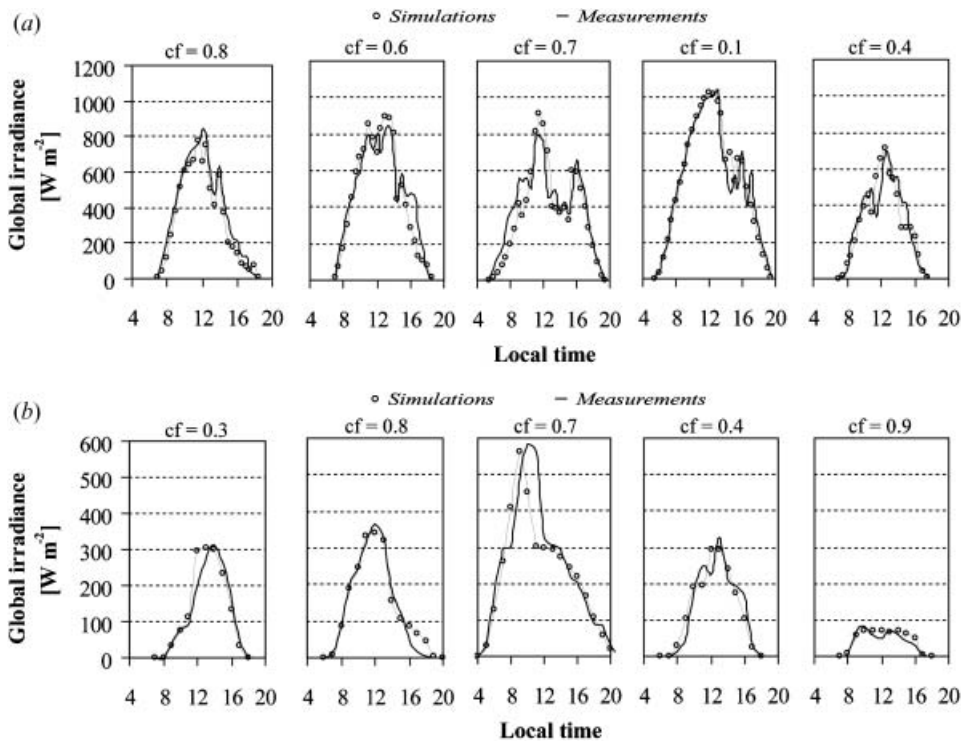


Figure 9. Diurnal comparisons of hourly global solar irradiance estimates and measurements from the Kendall (a) and Koege (b) validation sites during variable degrees of cloudiness. The daily mean cloud fraction (cf) within the diffuse source area of the sites is indicated for each of the selected days.

satellite estimates were converted to hourly averages using an appropriate weighting technique; and only hours with a Sun elevation >0 during the entire hour were kept for the analysis. The comparisons were done using the average value of a 2×2 block (10×10 km) around the corresponding validation sites, since the geographic location of the stations may not be in the middle of a single pixel. Overall validation results are presented in table 2 in terms of the root mean square deviation (RMSD), mean deviation (MD) and mean absolute bias deviation (MABD) expressed as a percentage of the average measured global irradiance and in units of W m^{-2} . For Southern Arizona, hourly global solar irradiance data were retrieved with an overall RMSD of 11.5% (59.5 W m^{-2}) and an MABD of 0.7% (3.8 W m^{-2}), while a RMSD of 26.6% (71.6 W m^{-2}) and a MABD of 1.3% (3.5 W m^{-2}) were characteristic for the Island of Zealand (table 2).

Deviations between satellite estimates and surface measurements decrease as the integration time increases, as visualized in figure 10 for daily mean global solar irradiance values resulting in overall RMSDs of 5.8% and 13.4% for Southern Arizona (figure 10(a)) and the Island of Zealand (figure 10(b)), respectively.

The much higher RMSDs reported for the Island of Zealand are not necessarily a result of degraded accuracy but more likely a reflection of the local cloud environment and frequency of cloud cover, which may affect the comparability between satellite estimates and ground observations. Satellite estimates differ fundamentally from point measurements made by pyranometers in terms of

Table 2. Overall root mean square deviations (RMSD), mean deviations (MD), and mean absolute bias deviations (MABD) for all-sky global solar irradiance for the two study regions.

		RMSD		MD		MABD	
		%	W m^{-2}	%	W m^{-2}	%	W m^{-2}
Arizona	Hourly	11.5	59.5	8.3	43.3	0.7	3.8
	Overpass	12.3	63.0	9.0	46.0	0.8	4.0
	Daily mean	5.8	27.0	4.5	20.9	0.9	3.9
Denmark	Hourly	26.6	71.6	18.9	51.5	1.3	3.5
	Overpass	22.1	75.2	15.9	54.0	1.6	5.3
	Daily mean	13.4	28.7	10.3	22.2	1.9	4.1

The statistics are reported in absolute (W m^{-2}) and relative units (percentage of average measured global irradiance) for hourly and daily mean solar irradiance data. The performance of the hourly simulations closest to the time of the Terra and Agua overpasses is also given. The MABD is computed as the absolute average of the mean bias deviation (MBD) for each validation site. The statistic equations used are given below.

$$e = \text{satellite predictions}; m = \text{tower measurements}; \text{MD} = 100 \cdot \frac{1}{n} \sum_1^n |e - m| \bigg/ \frac{1}{n} \sum_1^n m; \text{MABD} = 100 \cdot \frac{1}{n} \sum_1^n (e - m) \bigg/ \frac{1}{n} \sum_1^n m; \text{RMSD} = 100 \cdot \sqrt{\frac{1}{n} \sum_1^n (e - m)^2} \bigg/ \frac{1}{n} \sum_1^n m.$$

sampling frequency and observational scale. Satellite estimates provide an areal average at an instant in time, while pyranometers make measurements every 2–10 s at a single point. As a consequence, large spatial gradients in solar irradiance fields will reduce the comparability of satellite estimates and surface point measurements and result in higher RMSDs. Thus, reported RMSDs will be specific for the region being studied and not directly indicative of the actual model performance (Zelenka *et al.* 1999).

The degree of spatial variability in solar irradiance for a given region can be deduced by plotting the relative RMSDs between measurements from pairs of

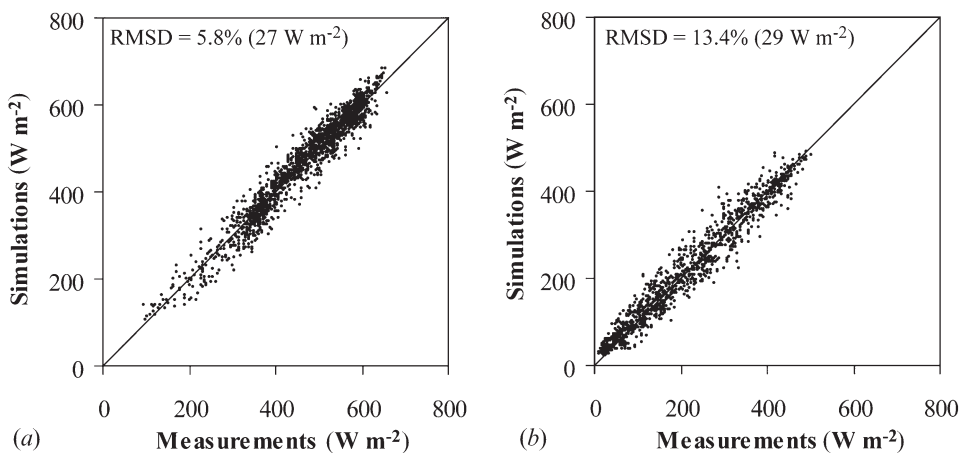


Figure 10. Scatter plots of daily mean measured and estimated global solar irradiance from all validation sites within Southern Arizona (a) and the Island of Zealand (b). The diurnal satellite and ground truth datasets were converted to daily mean datasets by appropriately averaging the hourly observations based on the time of sunrise and sunset.

network sites as a function of distance between the sites (Perez *et al.* 1997, Zelenka *et al.* 1999). For Southern Arizona, the RMSDs between neighbouring ground measurements reach 11–15% within a distance of 10–15 km between the network sites, while RMSDs as high as 23–29% are reached within the same distance for the Island of Zealand (figure 11). The high frequency of clear skies for Southern Arizona, which causes homogeneous solar irradiance fields, is the main reason for the comparably low RMSDs. For both regions, the satellite-derived estimates are seen to be more reliable than measurements from a neighbouring site if the network site operates further away than approximately 15 km from the point of interest, indicating similar global solar irradiance accuracy levels for the two regions despite the large difference in the RMSDs. With the same line of reasoning, the observed deviations compare favourably to the performances of approaches using geostationary satellites that have suggested the use of satellite derived solar irradiance data rather than measurements from a neighbouring site if the latter operates further away than 20–30 km from the site (Perez *et al.* 1997). For a daily integration time, the reported RMSDs of 5.8 and 13.4% are reached within a distance of approximately 50 km for Southern Arizona and 25 km for the Island of Zealand (figure 11).

The model performance was also evaluated by comparison with solar irradiance retrieval accuracies reported in the literature for similar climatic regions. Based on GOES-8 satellite data, Perez *et al.* (2002) reported hourly RMSDs in the order of 10–16% for arid localities in New Mexico and California, while Stewart *et al.* (1999) reported an overall RMSD of 16.8% and a bias of 6.4% for a coastal plain near Ciudad Obregon in the arid environment of North-western Mexico. Using GOES or METEOSAT imagery, Ineichen and Perez (1999) obtained a precision in the order of 30% for mid-latitude sites in Europe and USA characterized by a much higher percentage of sunshine hours than Denmark ($\approx 60\%$ versus $\approx 35\%$). Few authors have reported hourly estimates for northern latitudes, but Olseth and Skartveit

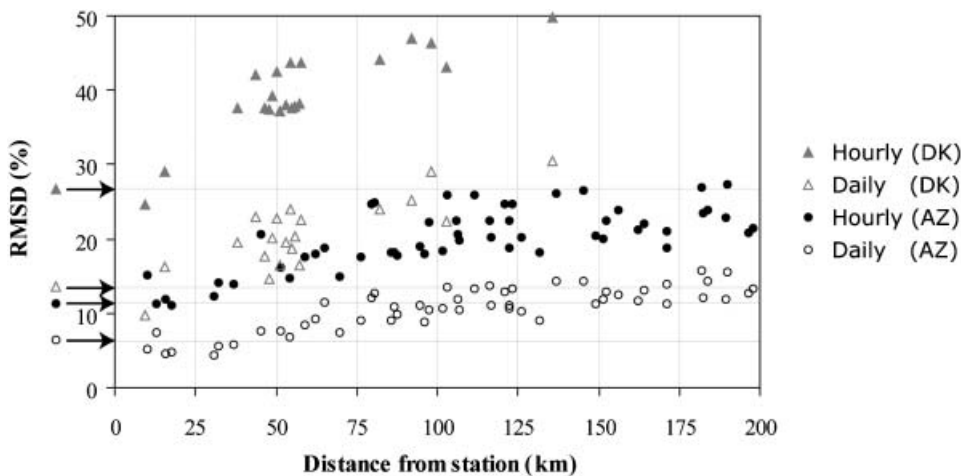


Figure 11. Relative RMSDs between global solar irradiance measurements from pairs of network sites as a function of the distance between the sites. All validation sites shown on figure 1 were used in the analysis. The satellite retrieval accuracies indicated by arrows on the *y*-axis demonstrate that the satellite-derived estimates are more reliable than measurements from a neighbouring site if the distance from the point of interest to the network site is more than approximately 15 km for hourly and 25–50 km for daily integration times.

(2001) obtained an RMSD of 25% for the site of Bergen (60.4° N, 5.3° E) using METEOSAT data, while Laine *et al.* (1999) reported a standard error of 28% between instantaneous estimates based on AVHRR imagery and 15-min average pyranometer measurements from six Finish stations (60° N to 69° N). These comparisons provide confidence in the applied methodology and demonstrate the feasibility of using a morning and afternoon MODIS overpass in combination with a cloud-tracking scheme for hourly estimates of global solar irradiance throughout the day.

3.4 Sources of uncertainty

A detailed statistic analysis of the hourly global solar irradiance estimates is given in figure 12 that shows the variation of seasonal biases and RMSDs and the range in these statistics between the validation sites. For Southern Arizona, the annual RMSD is seen to range from 10 to 14.7% between the validation sites, which hides a large seasonal and between-station variability (figure 12(a)). The biases are fairly consistent from season to season with maximum deviations of 8% (September) and -7% (December). For the Island of Zealand, the largest relative RMSDs occur during the winter months, which are characterized by a low radiation environment (figure 12(b)). The low annual mean bias deviations are seen to hide some seasonal effects, with January standing out as most problematic with a regional MBD of -16% (figure 12(b)). The model under-predictions for January may be attributed to errors in the surface albedo. Due to insufficient high-quality cloud free MODIS reflectances for the month of January (3.5 percentage of sunshine hours), the MODIS albedo retrievals rely on a less accurate backup algorithm based on database values. Additionally, the 16-day albedo product will not be able to capture fluctuations caused by occasional snow cover that typically last less than a week for this environment. In light of the sensitivity results (figure 5(a)), these factors (in addition to inadequate information on the atmospheric state during overcast conditions) may easily explain the January bias in addition to the overall tendency for larger biases during the winter months.

The monthly variations in the RMSDs can be attributed to a number of factors such as the frequency of clear skies and the cloud cover conditions that may be characterized by spatially uniform stratiform type of clouds or complex convective

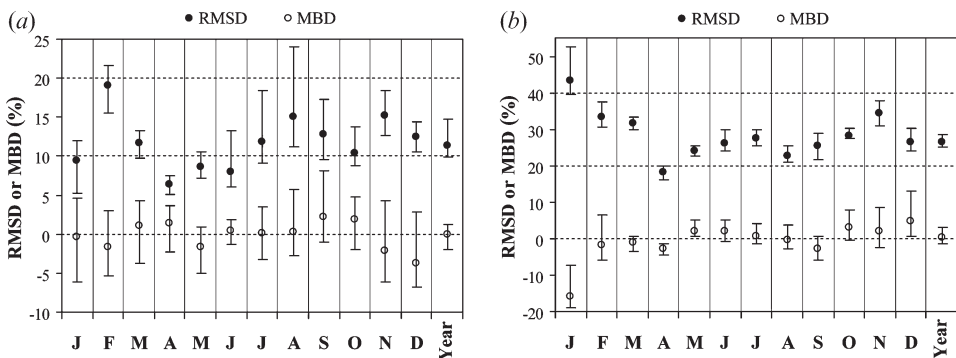


Figure 12. Seasonal variation of overall mean bias deviations (MBD) and root mean square deviations (RMSD) for Southern Arizona (a) and the Island of Zealand (b). The error bars represent the range in the statistics observed between the validation sites.

type clouds exhibiting large variations in cloud optical thickness. The latter is typically for the Arizona monsoon season (July to September) and the Danish summer months, while frontal cloud systems are typical for the remainder of the year with a much higher frequency for the Danish region.

Plots of daily mean RMSDs as a function of the daily mean cloud fraction (from sunrise to sunset) within the diffuse source area of the validation sites illustrate the contrasting cloud environments of the two regions with cloud fractions less than 0.3 occurring on 64% and 27% of the days for Southern Arizona (figure 13(a)) and the Island of Zealand (figure 13(b)), respectively. At the same time, overcast conditions on a daily timescale are rare for Southern Arizona (1%) while common for the Island of Zealand (20%). The RMSDs are seen to increase steadily with increasing cloud fraction reaching maximum values of 14% and 29%, respectively, while absolute RMSDs are comparable, ranging from 20 to 40 $W m^{-2}$. For Southern Arizona as a whole, the model tends to slightly overpredict solar irradiances during clear sky conditions (MBD=1.3%), while the model underpredicts during partly cloudy and overcast conditions (MBD=-1 to -5%).

The tendency of the model to overestimate clear sky solar irradiance for Southern Arizona contradicts with the positively biased AOD retrievals (figure 6(a)) that induce a decrease in solar irradiance (figure 5(b)) and could indicate a cancellation of errors in the clear sky model. Even though rural aerosol model parameterizations of the asymmetry factor and single-scattering albedo may be inappropriate for a semi-arid environment, they are consistent with ground observations at the semi-arid site of Tombstone, Arizona (Pinker *et al.* 2004). Likewise, the MODIS derived Angström exponents agree reasonably with AERONET measurements from the Maricopa site with a bias of 0.11 (not shown) that cannot offset the clear-sky solar irradiance underestimation of 6–25% caused by using the biased AOD values (figure 6(a)). A possible reason for the positively biased clear sky model estimates may be undetected cirrus clouds as a result of the poor cirrus detection capabilities of the MODIS cloud-detection algorithm (<http://modis-atmos.gsfc.nasa.gov/validation.html>) or dust storms, both of which are common occurrences in this region.

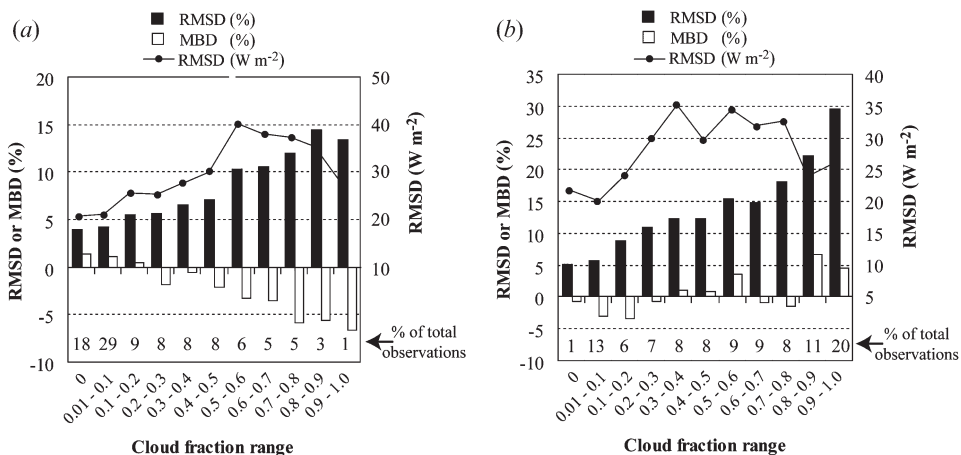


Figure 13. Overall RMSDs and MBDs for daily mean satellite estimates of global solar irradiance depicted as a function of daily mean cloud fraction ranges based on data from all validation sites within Southern Arizona (a) and the Island of Zealand (b). The percentage of observations within each cloud fraction range is listed below the columns.

The poor MODIS AOD retrieval results for the semi-arid environment of Southern Arizona suggest the use of supporting data sources such as the AERONET ground-based aerosol climatology (Holben *et al.* 2001) and the Model of Atmospheric Transport and Chemistry, MATCH (http://www.cgd.ucar.edu/cms/match/new_website/). Aerosol transport models like MATCH may also provide useful aerosol information during overcast conditions where satellite predictions are unavailable.

TPW values based on the MODIS near-infrared retrieval algorithm were an excellent source for describing horizontal gradients (figure 7). Still, a coupling with ancillary water vapour content data from weather prediction models (e.g. NCEP and ECMWF) or the all-sky TPW product from the Atmospheric Infrared Sounder (AIRS) onboard the Aqua satellite may be envisaged for an improved description of TPW for all-sky conditions.

3.4.1 Cloud information. The cloud optical thickness is by far the most critical parameter (figure 5(a)). The COT retrieval algorithm should work well for horizontally homogeneous and single-layer cases, while incorrect retrievals are likely for pixels that encounter multiple-layer or horizontally inhomogeneous cloud structures (King *et al.* 1997). Unsatisfactory results will also occur for large Sun zenith angles due in part to increased probability of shadows and complex 3D cloud effects, and large Sun zenith angles could be another possible explanation for the somewhat higher biases observed during the Danish winter months (figure 12(b)). Uncertainties in determining the COT can also be ascribed to the inaccuracy associated with the atmospheric correction.

A strong dependence of the solar irradiance retrieval accuracy on the spatial variability in COT is evident from figure 14. For the Island of Zealand, the RMSDs are seen to vary from the clear sky estimate of 4.4% to 62% during conditions when the COT standard deviation is greater than 20 (figure 14(b)). This tendency is partly

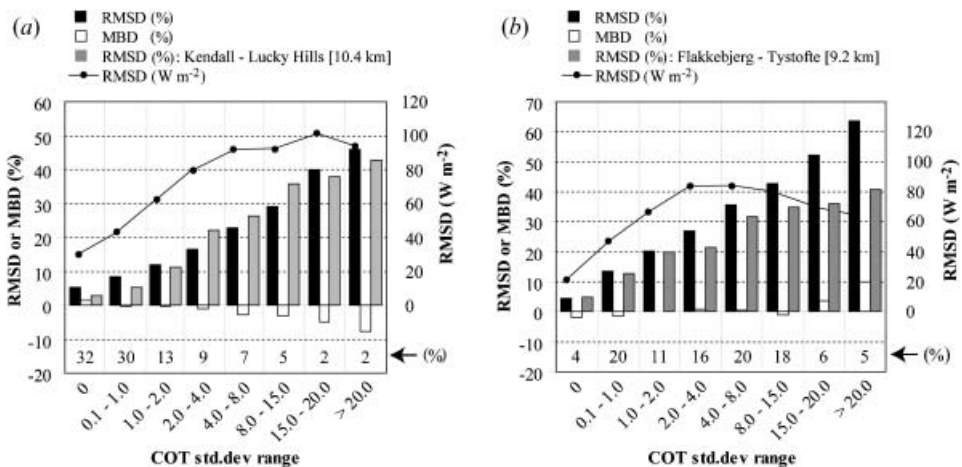


Figure 14. Overall RMSDs and MBDs for hourly satellite estimates of global solar irradiance depicted as a function of the spatial variability (the standard deviation) in the cloud optical thickness (COT) based on data from all validation sites within Southern Arizona (a) and the Island of Zealand (b). The relative RMSD between measurements from network sites approximately 10 km apart is shown for comparison. The percentage of observations within each COT standard deviation (std.dev) range is listed below the columns.

related to the increasing complexity and heterogeneity of the cloud masses and the occurrences of broken cloud conditions, which cause highly non-stationary solar irradiance fields and reduced comparability between point-based pyranometer measurements and areal averaged satellite estimates. As a consequence, the relative RMSD between solar irradiance measurements from pairs of network stations only 10 km apart reaches a value of around 40% at COT standard deviations greater than 20 (figure 14(a) and (b)).

The increase in RMSDs is also related to uncertainties in the cloud-tracking scheme as the accurate positioning of cloud information in time and space becomes increasingly important as the spatial gradients in the COT steepen. For instance, an error of 3 m s^{-1} in the cloud drift vectors induces a cloud information displacement of 11 km for every hour away from the satellite overpass time, which can have large implications for the accuracy of the solar irradiance estimates for heterogeneous cloud cover conditions. Nevertheless, the simplifying assumptions of the cloud-tracking scheme (§2.3.3) seem to be acceptable for the study regions, considering the rather comparable RMSDs of the all-day hourly simulations and the simulations closest to the overpasses (table 2).

3D cloud effects may also impact the accuracy of the satellite estimates especially for convective cloud cover conditions and in the case of pronounced vertical structures in the cloud field (Wyser *et al.* 2002). However, the applied averaging of cloud information within the direct-beam and diffuse source area of each pixel (§2.3.4) is believed to account for some of these radiative effects.

4. Conclusion

The applicability of MODIS imagery for the mapping of temporally and spatially distributed fields of all-sky global solar irradiance was demonstrated for the semi-arid environment of Southern Arizona, USA and for a Northern European region located in the zone of prevailing westerlies. For both regions, the satellite-derived estimates of hourly global solar irradiance were shown to be more reliable than measurements from a nearby ground station if the latter operates further away than 15 km from the point of interest being comparable to the accuracy level obtainable from geostationary satellites.

The solar irradiance estimates were retrieved by combining a neural network and a clear-sky radiative transfer model implemented with MODIS derived clear-sky atmospheric state and cloud optical and radiative parameters.

A validation of MODIS atmospheric state data against AERONET measurements demonstrated the usefulness of the data for the delineation of spatial gradients during clear-sky conditions. However, large biases were associated with the aerosol optical depth retrievals for the semi-arid region, while total precipitable water vapour retrievals, based on the MODIS near-infrared algorithm, were characterized by systematic deviations from the measurements. These factors of uncertainty in addition to the clear-sky restriction of the MODIS retrievals resulted in inadequate descriptions of the atmospheric state for the semi-arid region and during overcast conditions. As a result, further model improvements call for a combination of atmospheric state data provided by MODIS and satellite sensors such as the Atmospheric Infrared Sounder (AIRS), weather prediction models, climatologies, or aerosol transport and chemistry models.

The utilization of MODIS data from two overpasses during the daytime in association with a cloud-tracking scheme made hourly estimates of global solar

irradiance feasible from the time of sunrise until sunset. The application of cloud motion vectors inevitably leads to additional errors due to uncertainties related to the position of cloud elements in time and space and the violation of the assumption of complete shape coherence of cloud elements. As a result, higher retrieval accuracies were reported during periods of relatively homogeneous cloud conditions, characterized by a low spatial variability in the cloud optical thickness, than those observed during conditions of steep spatial gradients in cloud optical thickness. Despite the obvious limitations of the cloud vector methodology, the encouraging hourly verification results reported for diverse cloud conditions and environments provide confidence in the approach.

The proposed scheme can provide significantly improved maps of hourly and daily mean solar irradiances in regions with sparse meteorological observations and in high latitudes where data from geostationary satellites are either unavailable or of low quality, and the overpasses of the Terra and Aqua satellites become more frequent. The availability of three or more overpasses during the daytime above approximately 60° latitude will probably improve the solar irradiance estimates in these regions even further. Overall improvements in solar irradiance mapping may also be envisaged by a synergistic use of polar orbiting and geostationary satellites. Benefits of using MODIS are related to its good cloud characterization and retrieval capabilities at unprecedented spatial resolutions that permit the integrated use of accurate radiative transfer schemes.

Future work will focus on the validation of derived direct-beam and diffuse solar irradiance components and on the integration of atmospheric state data from ancillary data sources. Additionally, the scheme will utilize the significantly improved MODIS collection 5 datasets that become available in the very near future (http://modis-atmos.gsfc.nasa.gov/products_C005update.html).

Acknowledgements

The present study was funded by the Danish Natural Science Research Council (grant no. 21-04-0499) and the Nordic Centre for Studies of Ecosystem Carbon Exchange and its Interactions with the Climate System (NECC). We would like to acknowledge the Arizona Meteorological Network (AZMET) and the Southwest Watershed Research Center (SWRC) for making valuable validation data of global solar irradiance available. We would also like to acknowledge the PIs of the Maricopa and Gotland AERONET sites and Jeff Key for providing the *Fluxnet* source code.

References

- ACKERMAN, S.A., STRABALA, K.I., MENZELL, W.P., FREY, R.A., MOELLER, C.C. and GUMLEY, L.E., 1998, Discriminating clear sky from clouds with MODIS. *Journal of Geophysical Research*, **103**, pp. 32141–32157.
- BA, M.B., FROUIN, R., NICHOLSON, S.E. and DEDIEU, G., 2001, Satellite-derived surface radiation budget over the African continent. Part 1: estimation of downward solar irradiance and albedo. *Journal of Climate*, **14**, pp. 45–58.
- BEYER, H., COSTANZO, C. and HEINEMAN, D., 1996, Modifications of the heliosat procedure for irradiance estimates from satellite images. *Solar Energy*, **56**, pp. 207–212.
- BIRD, R.E. and RIORDAN, C.J., 1986, Simple simple solar spectral model for direct and diffuse irradiance on horizontal and tilted planes at the earth's surface for cloudless atmospheres. *Journal of Climate and Applied Meteorology*, **25**, pp. 87–97.

- BISHOP, J.K.B. and ROSSOW, W.B., 1991, Spatial and temporal variability of global surface solar irradiance. *Journal of Geophysical Research*, **96**, pp. 16839–16858.
- CEBALLOS, J.C., BOTTINO, M.J. and DE SOUZA, J.M., 2004, A simplified physical model for assessing solar radiation over Brazil using GOES 8 visible imagery. *Journal of Geophysical Research*, **109**, D02211, doi: 10.1029/2003JD003531.
- CANO, D., MONGET, J.M., ALBUISSON, M., GUILLARD, H., REGAS, N. and WALD, L., 1986, A method for the determination of the global solar radiation from meteorological satellite data. *Solar Energy*, **37**, pp. 31–39.
- DENMARK'S METEOROLOGICAL INSTITUTE 2006, Available online at: www.dmi.dk (accessed 1 May 2006).
- DIAK, G.R., BLAND, W.L. and MECIKALSKI, J., 1996, A note on first estimates of surface insolation from GOES-8 visible satellite data. *Agricultural and Forest Meteorology*, **82**, pp. 219–226.
- GAO, B.-C. and KAUFMAN, Y.J., 2003, Water vapor retrievals using Moderate Resolution Imaging Spectroradiometer (MODIS) near-infrared channels. *Journal of Geophysical Research*, **108**, 4389, doi: 10.1029/2002JD003023.
- GAUTIER, C., DIAK, G. and MASSE, S., 1980, A simple model to estimate the incident solar radiation at the surface from GOES satellite data. *Journal of Applied Meteorology*, **19**, pp. 1005–1012.
- GAUTIER, C. and LANDSFIELD, M., 1997, Surface solar radiation flux and radiative forcing for the Atmospheric Radiation Measurement (ARM) Southern Great Plains (SGP): A satellite, surface observations, and radiative transfer model study. *Journal of Atmospheric Sciences*, **54**, pp. 1289–1307.
- HOLBEN, B.N., ECK, T.F., SLUTSKER, I., TANRE, D., BUIS, J.P., SETZER, A., VERMOTE, E., REAGAN, J.A., KAUFMAN, Y., NAKAJIMA, T., LAVENU, F., JANKOWIAK, I. and SMIRNOV, A., 1998, AERONET—a federated instrument network and data archive for aerosol characterization. *Remote Sensing of Environment*, **66**, pp. 1–16.
- HOLBEN, B.N., TANRE, D., SMIRNOV, A., ECK, T.F., SLUTSKER, I., ABUHASSAN, N., NEWCOMB, W.W., SCHAFER, J.S., CHATENET, B., LAVENU, F., KAUFMAN, Y.J., CASTLE, J.V., SETZER, A., MARKHAM, B., CLARK, D., FROUIN, R., HALTHORE, R., KARNALI, A., O'NEILL, N.T., PIETRAS, C., PINKER, R.T., VOSS, K. and ZIBORDI, G., 2001, An emerging ground-based aerosol climatology: Aerosol optical depth from AERONET. *Journal of Geophysical Research*, **106**, pp. 12067–12097.
- IAMAP 1986, *A Preliminary Cloudless Standard Atmosphere for Radiation Computation, Rep. WCP-112, WMO/ID-No. 24* (Geneva: World Meteorological Organization).
- INEICHEN, P. and PEREZ, R., 1999, Derivation of cloud index from geostationary satellites and application to the production of solar irradiance and daylight illuminance data. *Theoretical and Applied Climatology*, **64**, pp. 119–130.
- JACOBS, J.M., MYERS, D.A., ANDERSON, M.C. and DIAK, R.D., 2002, GOES surface insolation to estimate wetlands evapotranspiration. *Journal of Hydrology*, **266**, pp. 53–65.
- JUSTUS, C.G. and PARIS, M.V., 1984, A model for solar spectral irradiance and radiance at the bottom and top of a cloudless atmosphere. *Journal of Applied Meteorology*, **24**, pp. 193–205.
- KAUFMAN, Y.J. and GAO, B.C., 1992, Remote sensing of water vapor in the near IR from EOS/MODIS. *IEEE Transactions on Geoscience and Remote Sensing*, **30**, pp. 871–884.
- KAUFMAN, Y.J., TANRE, D., REMER, L.A., VERMOTE, E.F., CHU, A. and HOLBEN, B.N., 1997, Operational remote sensing of tropospheric aerosol over land from EOS moderate resolution imaging spectroradiometer. *Journal of Geophysical Research*, **102**, pp. 17051–17067.
- KAUFMAN, Y.J., HERRING, D.D., RANSON, K.J. and COLLATZ, G.J., 1998, Earth observing system AM1 mission to earth. *IEEE Transactions on Geoscience and Remote Sensing*, **36**, pp. 1045–1055.

- KEY, J. and SCHWEIGER, A.J., 1998, Tools for atmospheric radiative transfer: *Streamer* and *FluxNet*. *Computers and Geosciences*, **24**, pp. 443–451.
- KEY, J., AMANO, E., COLLINS, J. and SCHWEIGER, A., 2001, *FluxNet User's Guide* (Madison: Cooperative Institute for Meteorological Satellite Studies, University of Wisconsin).
- KEY, J., 2002, *The Cloud and Surface Parameter Retrieval (CASPR) System for Polar AVHRR User's Guide* (Madison: Cooperative Institute for Meteorological Satellite Studies, University of Wisconsin).
- KING, M.D., TSAY, S.-C., PLATNICK, S.E., WANG, M. and LIOU, K.-N., 1997, Cloud retrieval algorithms for MODIS: optical thickness, effective particle radius, and thermodynamic phase. MODIS Algorithm Theoretical Basis Document No. ATBD-MOD-05, MOD06—Cloud product. Available online at: http://modis-atmos.gsfc.nasa.gov/_docs/atbd_mod05.pdf (accessed 1 May 2006).
- KING, M.D., MENZEL, W.P., KAUFMAN, Y.J., TANRÉ, D., GAO, B.C., PLATNICK, S., ACKERMAN, S.A., REMER, L.A., PINCUS, R. and HUBANKS, P.A., 2003, Cloud and Aerosol Properties, Precipitable Water, and Profiles of Temperature and Water Vapor from MODIS. *IEEE Transactions on Geoscience and Remote Sensing*, **41**, pp. 442–456.
- LAINÉ, V., VENÄLÄINEN, A., HEIKINHEIMO, M. and HYVÄRINEN, O., 1999, Estimation of surface solar global radiation from NOAA AVHRR data in high latitudes. *Journal of Applied Meteorology*, **38**, pp. 1706–1719.
- MEEUS, J., 1991, *Astronomical Algorithms* (Richmond, VA: Willmann-Bell).
- MENZEL, W.P., 2001, Cloud tracking with satellite imagery: from the pioneering work of Ted Fujita to the present. *Bulletin of the American Meteorological Society*, **82**, pp. 33–47.
- MENZEL, W.P., SEEMAN, S.W., LI, J. and GUMLEY, L.E., 2002, MODIS atmospheric profile retrieval algorithm theoretical basis document. MODIS ATBD. Available online at: <http://modis-atmos.gsfc.nasa.gov> (accessed 1 May 2006).
- NIEMAN, S.J., MENZEL, W.P., HAYDEN, C.M., GRAY, D., WANZONG, S., VELDEN, C. and DANIELS, J., 1997, Fully automated cloud-drift winds in NESDIS operations. *Bulletin of the American Meteorological Society*, **78**, pp. 1121–1133.
- OLSETH, J.A. and SKARTVEIT, A., 2001, Solar irradiance, sunshine duration and daylight illuminance derived from METEOSAT data for some European sites. *Theoretical and Applied Climatology*, **69**, pp. 239–252.
- PEREZ, R., SEALS, R. and ZELENKA, A., 1997, Comparing satellite remote sensing and ground network measurements for the production of site/time specific irradiance data. *Solar Energy*, **60**, pp. 89–96.
- PEREZ, R., INEICHEN, P., MOORE, K., KMIECIK, M., CHAIN, C., GEORGE, R. and VIGNOLA, F., 2002, A new operational model for satellite-derived irradiances: description and validation. *Solar Energy*, **73**, pp. 307–317.
- PINKER, R.T. and LASZLO, I., 1992, Modeling surface solar irradiance for satellite applications on a global scale. *Journal of Applied Meteorology*, **31**, pp. 194–211.
- PINKER, R.T., KUSTAS, W.P., LASZLO, I., MORAN, M.S. and HUETE, A.R., 1994, Basin-scale solar irradiance estimates in semiarid regions using GOES 7. *Water Resources Research*, **30**, pp. 1375–1386.
- PINKER, R., PANDIETHURAI, G., HOLDEN, B., KEEFER, T.O. and GOODRICH, D.C., 2004, Aerosol radiative properties in the semi-arid Western United States. *Atmospheric Research*, **71**, pp. 243–252.
- PLATNICK, S., KING, M.D., ACKERMAN, S.A., MENZEL, W.P., BAUM, B.A., RIÉDI, J.C. and FREY, R.A., 2003, The MODIS cloud products: algorithms and examples from Terra. *IEEE Transactions on Geoscience and Remote Sensing*, **41**, pp. 459–473.
- REMER, L.A., KAUFMAN, Y.J., TANRÉ, D., MATTOO, S., CHU, D.A., MARTINS, J.V., LI, R.R., ICHOKU, C., LEVY, R.C., KLEIDMAN, R.G., ECK, T.F., VERMOTE, E. and HOLBEN, B.N., 2005, The MODIS aerosol algorithm, products, and validation. *Journal of the Atmospheric Sciences*, **62**, pp. 947–973.

- RIGOLLIER, C., LEFÈVRE, M. and WALD, L., 2004, The method Heliosat-2 for deriving shortwave solar radiation data from satellite images. *Solar Energy*, **77**, pp. 159–169.
- SEEMANN, S.W. and LI, J., 2003, Operational retrieval of atmospheric temperature, moisture, and ozone from MODIS infrared radiances. *Journal of Applied Meteorology*, **42**, pp. 1072–1091.
- SKARTVEIT, A., OLSETH, J.A. and TUFF, M.E., 1998, An hourly diffuse fraction model with correction for variability and surface albedo. *Solar Energy*, **63**, pp. 173–183.
- STAMNES, K., TSAY, S.C., WISCOMBE, W. and LASZLO, I., 2000, *A General-Purpose Numerically Stable Computer Code for Discrete-Ordinate-Method Radiative Transfer in Scattering and Emitting Layered Media*, DISORT Report v1.1.
- STEWART, J.B., WATTS, C.J., RODRIGUEZ, J.C., DE BRUIN, H.A.R., VAN DEN BERG, A.R. and GARATUZA-PAYÁN, J., 1999, Use of satellite data to estimate radiation and evaporation for northwest Mexico. *Agricultural Water Management*, **38**, pp. 181–193.
- VERMOTE, E.F., EL SALEOUS, N.Z. and JUSTICE, C.O., 2002, Atmospheric correction of MODIS data in the visible to middle infrared: first results. *Remote Sensing of Environment*, **83**, pp. 97–111.
- WOLFE, R.E., ROY, D.P. and VERMOTE, E., 1998, MODIS land data storage, gridding and compositing methodology: Level 2 Grid. *IEEE Transactions on Geoscience and Remote Sensing*, **36**, pp. 1324–1338.
- WOLFE, R.E., NISHIHAMA, M., FLEIG, A.J., KUYPER, J.A., ROY, D.P., STOREY, J.C. and PATT, F.S., 2002, Achieving sub-pixel geolocation accuracy in support of MODIS land science. *Remote Sensing of Environment*, **83**, pp. 31–49.
- WYSER, K., O'HIROK, W., GAUTIER, C. and JONES, G., 2002, Remote sensing of surface solar irradiance with corrections for 3-D cloud effects. *Remote Sensing of Environment*, **80**, pp. 272–284.
- ZELENKA, A., PEREZ, R., SEALS, R. and RENNE, D., 1999, Effective accuracy of satellite derived hourly irradiances. *Theoretical and Applied Climatology*, **62**, pp. 199–207.
- ZHANG, Y.-C., ROSSOW, W.B. and LACIS, A.A., 1995, Calculation of surface and top-of-atmosphere radiative fluxes from physical quantities based on ISCCP datasets, Part I: method and sensitivity to input data uncertainties. *Journal of Geophysical Research*, **100**, pp. 1149–1165.